Identification, quantification and sourcing of fossil hydrocarbons in ancient Egyptian mummies by V and Ni trace elements

Océane Anduze, Didier Gourier, Laurent Binet, Alex Malergue, Vincent Grossi, Agnès Lattuati-Derieux

Identification, quantification and sourcing of fossil hydrocarbon in ancient Egyptian mummies by V and Ni trace elements

Océane Anduze,[a,b] Didier Gourier*[a,b] Laurent Binet,[a,b] Alex Malergue,[c] Vincent Grossi,[d] Agnès Lattuati-Derieux,[b,a]

[a] Chimie-ParisTech, PSL University, CNRS, Institut de Recherche de Chimie-Paris (IRCP), F-75005 Paris, France

[b] Centre de Recherche et de Restauration des Musées de France (C2RMF), Palais du Louvre, F-75001 Paris, France

[c] Université Côte d'Azur, CNRS, CEPAM, F-06000 Nice, France

[d] Aix Marseille Université, Université de Toulon, CNRS, IRD, Mediterranean Institute of Oceanography (MIO), F-13288 Marseille, France

*didier.gourier@chimieparistech.psl.eu

Egyptian mummies are often covered with a black embalming matter, which are made of complex mixtures of natural organic substances such as vegetable resins, beeswax, animal fats, gums, vegetable oils, as well as bitumen. In this work, we used Proton-induced X-ray emission (PIXE) and Electron Paramagnetic Resonance (EPR) to investigate the potential of certain transition metals, in particular V and Ni, as probes for detecting the presence of bitumen and tracing its origin and alteration in these black embalming matters. PIXE analysis showed that all the mummies studied in this work (birds, ram, crocodile, human), which span a period of about 1000 years and come from different sites in Egypt, have a nearly constant Ni/V ratio close to that of bitumen from the Dead Sea, suggesting a well-defined source of bitumen supply. The same conclusion was reached by EPR analysis of vanadyl porphyrins and carbonaceous radicals. The presence of an excess of radicals in the black matter from several mummies indicates that they probably contain some carbonized organic matter in addition to bitumen. This combined PIXE-EPR methodology is quantitative and sensitive since a few % of bitumen can be non-destructively detected in a mummy sample weighing only a few mg. The combination of these two techniques can provide new information on the thermal history (preparation recipes) and redox history (natural degradation) of these black matters.

Introduction

Mummies are among the most fascinating witnesses to the ancient Egyptians' beliefs about life after death. Their absolute need to preserve the body of the deceased from decay led the Egyptians to develop sophisticated mummification techniques. When the practice of embalming reached its most advanced level, during the New Kingdom, the mummification ritual was defined according to codified processes, comprising numerous steps.[1,2] Towards the end of the mummification ritual, when the body was drained and the thorax and abdominal cavities emptied of their organs, they were filled with tissues soaked in black matter, or simply with pure black matter.[3,4] Finally, the whole mummy was smeared with black matter before being wrapped in linen strips. Mummification was not just for humans, as millions of mummified mammals, birds and crocodiles have been buried in necropolises. They attest to the development of a cult of sacral animals, from the New Kingdom onwards and particularly during the Ptolemaic and Roman periods. The high demand for certain animal mummies, such as bird mummies for votive use, sold to people to accompany their prayers to the gods,[5] led to what can be described as industrial production.[6]

The embalming matter of Egyptian mummies result from a complex mixture of natural organic substances of various origins such as vegetable resins, beeswax, animal fats, gums, vegetable oils, pitches as well as bitumen.[7-13] Characterizing their composition is a major analytical challenge, as these amorphous organic materials are very heterogeneous and chemically degradable. Indeed, each individual substance of these natural matters is itself a complex blend of tens or hundreds of molecules belonging to a large range of chemical families. They are subject to various alteration processes linked to their manufacture (heating) and natural ageing (weathering, photooxidation, hydrolysis, biodegradation), and may present traces of ancient or recent (restoration, conservation, storage) contaminations. Last but not least, they are available only in very small quantities because they come from heritage objects or heritage human remains. In this context, the analytical molecular techniques using gas chromatography coupled with single quadrupole mass spectrometry (GC-MS), or Fourier transform infrared spectroscopy (FTIR), which have proved their relevance in archaeometry for determining the composition of complex organic archaeological materials,[14-16] are well adapted for analyzing the black matters of mummies, each type of substance being characterized by some biomarkers.[4,17-20]

Among all substances of animal and plant origins making up the black matters of mummies, bitumen has a special place because this fossil hydrocarbon material is more difficult to detect

and its use is rather recent, from the end of the New Kingdom (1250-1050 BC).[17] Bitumen is a geomaterial formed through a long geological process, that begins with the deposition on the sea floor of degraded biomolecular matter. After a long sequence of chemical transformations over millions of years, activated by the increase in temperature and pressure during burial, a part of this organic matter is transformed into oil and bitumen, which can either rise to the surface in free form, like the floating blocks of solid bitumen in the Dead Sea, or be trapped in rocks (oil sands, oil shale, etc.).[21-25] The presence of bitumen in embalming matter of mummies and other funerary objects has been demonstrated since the 90s by GC-MS analyses.[9,12,19] Among molecular markers of bitumen, steranes and hopanes are genuine molecular fossils, derived respectively from eukaryotic sterols and bacterial hopanoids in prokaryotic cells.[26] However, GC-MS requires preliminary extraction and fractionation steps, ruling out direct and non-destructive detection of bitumen. For this reason, the first protocols for molecular analysis of mummy black matters by GC-MS did not always take all these precautions into account, leading to a long-running controversy on the presence of bitumen in this material, pitting those who questioned its presence against those who claimed it.[7,17,27-33] Due to the relative complexity of these multi-step analytical procedures, the qualitative identification of bitumen in black matters by GC-MS can be difficult to achieve, especially when it is in low proportion. To overcome this difficulty, ^{14}C analysis can be used to estimate the amount of bitumen present in black matters. As the age of this fossil hydrocarbon material is measured in tens (or hundreds) of millions of years, its radiogenic ^{14}C isotope (half-life 5730 years) has long since disappeared. Thus, even a very small quantity of bitumen in the embalming matters of mummies affects their ^{14}C dating.[19]

In addition to the well-known sterane and hopane molecular biomarkers, bitumen is also characterized by its enrichment in certain transition metals which are present only at very low level in the sea and the environment. [21,22,34,35] Molybdenum (Mo) is the most abundant transition element in the ocean (~ 105 nmol/L), and serves as a paleoenvironmental proxy in organic sediments of marine origin.[34,36,37] Vanadium (V) and nickel (Ni) are less abundant in the ocean (~ 39 nmol/L and ~ 9 nmol/L, respectively).[22] However, organic sediments are enriched in these elements in the form of vanadyl porphyrins and nickel porphyrins (noted VO-P and Ni-P, respectively) trapped in asphaltenes, the most stable component of bitumen. These metal complexes can be considered as specific markers of bitumen,[35,38] due to their absence in the other biological components of the black matter, and are relatively resistant towards biodegradation.[39] Although V and Ni concentrations in bitumen may be affected by environmental weathering or biodegradation processes, the Ni/V ratio tends to remain constant

due to the similarity of the two metal complexes. For these reasons, both the presence of V, Ni and Mo enrichment and a specific Ni/V ratio should constitute reliable proxies for detecting the presence of bitumen in a complex bioorganic mixture such as embalming matter of mummies. Furthermore, nickel is in the Ni^{II} state over a wide range of *pH* and redox potential *Eh*, while V can be present in V^{V}, V^{IV} and V^{III} states depending on *Eh* and *pH* conditions ~~(Fig. S4)~~.[40,41] The determination of vanadium redox states in native bitumen and embalming matter can thus provide information on the environmental evolution of mummies (weathering, bio alteration …). Even if these metal elements are in low concentrations (tens to hundreds of $\mu g.g^{-1}$) in the black matter of mummies, they can be detected and quantified in a non-destructive way by X-ray emission spectroscopy. Moreover, a particularity of VO-P complexes is that they are paramagnetic (the V^{IV} state possesses an electron spin $S = 1/2$), so that they give a very characteristic signal in Electron Paramagnetic Resonance (EPR) spectroscopy.[42,43] Recently, EPR spectroscopy was used for a rapid and non-destructive detection of small amounts of bitumen in black matter of Egyptian mummies, when GC-MS had difficulty in detecting it.[44] The drawback is that only the V^{IV} state can be routinely detected by EPR. Nevertheless, the quantification of total vanadium ($V^{V}+V^{IV}+V^{III}$) by X-ray emission and of V^{IV} (in VO-P) by EPR should enable to partially trace the redox history of the mummies' bitumen.

In this work, we used Proton-Induced-X-ray Emission spectroscopy (PIXE) and EPR to analyze an homogeneous corpus of 14 mummies of birds, and another less homogeneous corpus made of human and animal mummies in which VO-P and carbonaceous radicals (hereafter referred to as C^0) were first identified by EPR.[44,45] Metal contents (V, Ni and Mo) were determined by PIXE, while vanadyl ions VO^{2+} characteristic of bitumen and C^0 radicals, present in all fossil hydrocarbon materials,[43,46] were quantified by EPR.

Materials and methods

Samples description and asphaltene isolation

A first corpus of samples, hereafter referred to as corpus A, consists of wrapping and feather fragments from 14 votive mummified birds in variable states of conservation. These fragments come from 7 birds of prey and 7 ibises from the *Musée des Confluences* (Lyon, France) and dating from the Third Intermediate period (~1077 BC to ~664 BC) to the Greco-Roman period (~310 BC to 476 AD).[6,47,48] Representative photographs of a mummified bird of prey and some samples studied by EPR and PIXE are shown in Fig.1. All the samples are described in Table S1 and their characteristics are reported in Table 1. A weighed sample taken from each

mummified bird was studied directly by EPR and PIXE without any preparation, and another sample was processed to extract the asphaltene component of bitumen which was analyzed by EPR. In this case, the samples were extracted with 4 mL of a 1:3 v/v methanol/dichloromethane mixture using ultrasonication conducted in an ultrasonic bath for 5 minutes. This step was repeated once. To achieve a complete extraction, the samples were then re-extracted with a 3:1 v/v dichloromethane/acetone mixture using ultrasonication conducted in an ultrasonic bath for 5 minutes. This step was also repeated once. The four extracts were gathered to provide the total organic extract. After evaporation under N_2 of the solvents, the total extract was dissolved in 500 µL of dichloromethane and 20 mL of heptane was then added slowly while maintaining magnetic stirring for 30 minutes. The sample was left overnight for decantation and then centrifuged (2 minutes, 3200 rpm) to separate the asphaltene precipitate from the solubilized extract. This latter was collected using a Pasteur pipette and the asphaltene precipitate was air-dried and collected for EPR analysis.

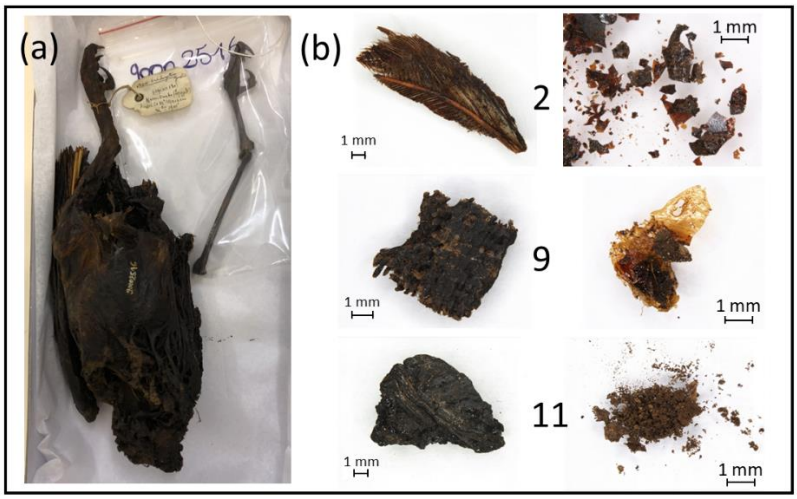

Fig. 1: (a) Photograph of a mummified bird of prey (sample 2 *Asio flammeus*, Ref: 90002516); (b) representative samples of feathers and wrapping covered with black matter (left) and their corresponding precipitates (right); from top to bottom: sample 2, sample 9 (*ibis*) (Ref: 90001245) and sample 11 (*ibis*) (Ref: 90010022); © Vincent Grossi and Alex Malergue. The bird mummies come from the *Musée des Confluences*, Lyon, France.

A second corpus of samples, hereafter referred to as corpus B (Table S2) was also analysed by PIXE and EPR in order to compare them with the birds of corpus A. These samples were previously analysed by different EPR methods,[44,45] and were taken from one human mummy (Hum2), a flow of black matter from the mummy's body covering the bottom of a coffin (Hum1), two rams (An1-3), a crocodile (An5), and fragments of a floating block of solid

bitumen from the Dead Sea (DS samples), which was the major source of bitumen in ancient Egypt funerary practices.[33,49,50]

Table 1: Characteristics of bird mummies from the collection of the *Musée des Confluences* (Lyon, France) analyzed by PIXE and EPR spectroscopy; The genera *Asio*, *Tyto*, *Micronisus*, *buteo* and *Circus* are birds of prey; the genera *Plegadis* and *Threskiornis* are two types of ibis. "Ind." means "indeterminate".

Sample	Reference	Type of bird	Site	Period	Dating
1	90002515	Asio otus	Kom Ombo	Ind.	Ind.
2	90002516	Asio flammeus	Kom Ombo	Roman period	30-40 AD
3	90002517	Tyto alba	Giza	Roman period	60 AD
4	90002518	Tyto alba	Giza	Roman period	58-68 AD
5	90010017	Threskiornis aethiopicus	Saqqarah	Late to Ptolem.	398-208 BC
6	90010018	Plegadis falcinellus	Saqqarah	3rd Int. period	831 BC
7	90002795	Micronisus gabar	Giza	Roman period	94 AD
8	90002801	Buteo vulpinus	Giza	Roman period	17-117 AD
9	90001245	Ibis *ind*	Kom Ombo	Ind.	Ind.
10	90010028	Threskiornis melanocephala	Kom Ombo	Ind.	Ind.
11	90010022	Ibis *ind*	Roda	Late period	534 BC
12	90010027	Ibis *ind*	Roda	Late to Ptolem.	517-341 BC
13	90010023	Ibis *ind*	Roda	Late to Ptolem.	405-200 BC
14	90010066	Circus pigargus	Roda	Ptolemaic	166 BC

Micro-PIXE measurements

Elemental measurements were carried out using Particle Induced X-ray Emission (PIXE)[51] at the *Accelerator Grand Louvre for Elemental Analysis* (AGLAE) of the C2RMF located in the Palais du Louvre, Paris. A 3 MeV proton micro-beam with a 5 nA intensity and a 50 µm diameter was used with four 50-mm^2 SDD-EDX detectors (Ketek AXAS-A). Three detectors were placed with an angle of 50° relative to the beam axis and screened with a 100 µm Mylar filter to collect X-rays from trace elements ($Z > 20$). An additional detector placed at 45°, without absorber and fitted with a magnetic deflector under a 1 L/min He flow, was used to record X-rays of light elements ($10 < Z < 29$), notably required for the trace elements calibration

(Fig.S1a). The simultaneous combination of three detectors with the same absorber is equivalent to a high solid angle super detector, increasing significantly the detection limit for trace elements without increasing irradiation doses (Fig.S1).[52] The hybrid scanning system included a fast vertical magnetic deflection of the beam as a 40×500 µm² brush across a 100-nm thick Si_3N_4 exit window, scanning the target surface as it was slowly mechanically translated. The samples, made up of organic matter, are probed to a depth of several tens of µm, which corresponds to both the penetration depth of the protons and the escape depth of the X-ray photons.

The data were obtained during two experimental measurement campaigns. Visually flat, roughly homogenous and black matter-rich areas were selected from photographs obtained with a binocular microscope on both sides of each sample studied. During the first campaign focused on the analysis of corpus B, large rectangular areas ranging from 2000×2000 µm^2 to 2500×3000 µm^2 were scanned with a pixel size of 25×25 µm² and a beam intensity ranging from 6 to 10 nA. During the second campaign, the raw samples from corpus A were scanned and new mappings were realized on selected samples from corpus B. The larger number of samples analyzed in the same limited time meant that the acquisition time per sample had to be reduced, so the rectangular areas were reduced to 1000×1000 µm^2. In addition, as part of a non-destructive approach, the irradiation dose was reduced as it proved sufficient for our analyses (beam intensity between 1 and 2 nA). The asphaltene precipitates from corpus A, in powder form, could not be analyzed by PIXE.

The small size of the samples was a difficulty (Tables S1 and S2), as AGLAE is designed to analyze medium-sized (a few centimeters) to large (a few meters) heritage objects. However, the spatial resolution of 25 µm enabled us to map a minimum area of 500×500 µm², on samples smaller than 1 mm. To analyze such small samples, we had to place them on a support topped by a plastiline cylinder covered with plastic film, so as to raise their surface vertically to the height of the AGLAE microbeam while avoiding any contamination of the samples (Fig. S1b). The AGLAE's camera was used to pinpoint the areas selected for analysis.

The collected PIXE spectra were extracted and processed by combining GUPIX, PyMca,[53] TrauPIXE and AGLAEmap softwares, the latter two having been developed at New AGLAE.[54] Details of the PIXE data treatment processing are described in SI section 2.1.

EPR measurements

EPR spectra were recorded at room temperature with a Bruker Elexsys E500 spectrometer operating at X-band (microwave frequency ≈ 9.4 GHz) equipped with a Bruker SHQE

resonator. The external magnetic field was modulated at 100 kHz for lock-in-detection, with a modulation amplitude of 0.2 mT for corpus A samples and 0.5 mT for corpus B samples. All spectra were recorded with a microwave power of 2 mW. All the samples (about 10-20 mg) were weighed and inserted without grinding into Suprasil EPR tubes for measurements, in order to preserve the integrity of the samples for subsequent analysis. Empty tubes spectra were recorded for background removal from experimental spectra. Spectra were simulated with the EasySpin toolbox for Matlab (version 5.2.28)[55] and with the spin Hamiltonian parameters measured on the experimental spectra.[44] The mass concentrations of C^0 and VO-P paramagnetic species were measured by comparing the experimental spectra with standard samples containing a known number of electron spins. We used a DPPH (diphenyl-picril-hydrazyl) standard containing $(3.7\pm0.4)\times10^{16}$ spins to measure the C^0 concentration, and a VOTPP (vanadyl tetraphenyl porphyrin) standard solution to measure VO-P concentration. All details of the procedures for measuring the EPR intensity and concentration are given in SI section 3.4.

Results and discussion

Quantification and sourcing of bitumen by PIXE analysis of V, Ni and Mo trace elements. Three examples of PIXE spectra are shown in Fig. 2, corresponding to a fragment of Dead Sea bitumen (DS sample), a fragment of black matter covering the bottom of a human coffin (sample Hum1, see Table S2), and a fragment of a bird-of-prey feather covered with black matter (sample 3, see Table S1). The experimental and simulated PIXE spectra of all the samples are shown in Figs. S2 and S3. To take into account the great chemical complexity of black matter and its biological supports, PIXE spectra were simulated taking into account 44 chemical elements from Na to U, but only the S_K, Ti_K, V_K, Cr_K, Ni_K and Mo_L transitions are indicated in Fig. 2. It can be seen that vanadium transitions overlap with those of other transition metals (see also Table S4). More precisely, $V_{K\alpha}$ transitions (4.94 keV) overlap with $Ti_{K\beta}$ transitions (4.93 keV), and $V_{K\beta}$ transitions (5.43 keV) overlap with $Cr_{K\alpha}$ transitions (5.41 keV). However, $Ti_{K\alpha}$ (4.51 keV) and $Cr_{K\beta}$ (5.95 keV) transitions are well separated from other elements, enabling independent measurement of Ti, V and Cr concentrations with good accuracy. $Ni_{K\alpha}$ (7.4 keV) and $Ni_{K\beta}$ (8.26 keV) transitions are isolated from transitions of other elements in DS bitumen, enabling accurate determination of Ni concentration. The determination of the Mo concentration is affected by a significant error because the $Mo_{L\alpha}$ transition (2.29 keV) partially overlaps with the intense $S_{K\alpha}$ transition at 2.31 keV ($S_{K\beta}$ occurs at 2.46 keV), as bitumen is always enriched in sulfur. Concentrations of Vanadium, nickel and

245 molybdenum (in µg.g^{-1}) are shown in Table 2 and Fig.3a. Concentrations of other elements are reported in Table S5. All concentrations were measured in visually homogeneous areas selected from PIXE mappings of samples from corpuses A and B. In two cases (An2 and Hum2), two mappings were performed on the same sample.

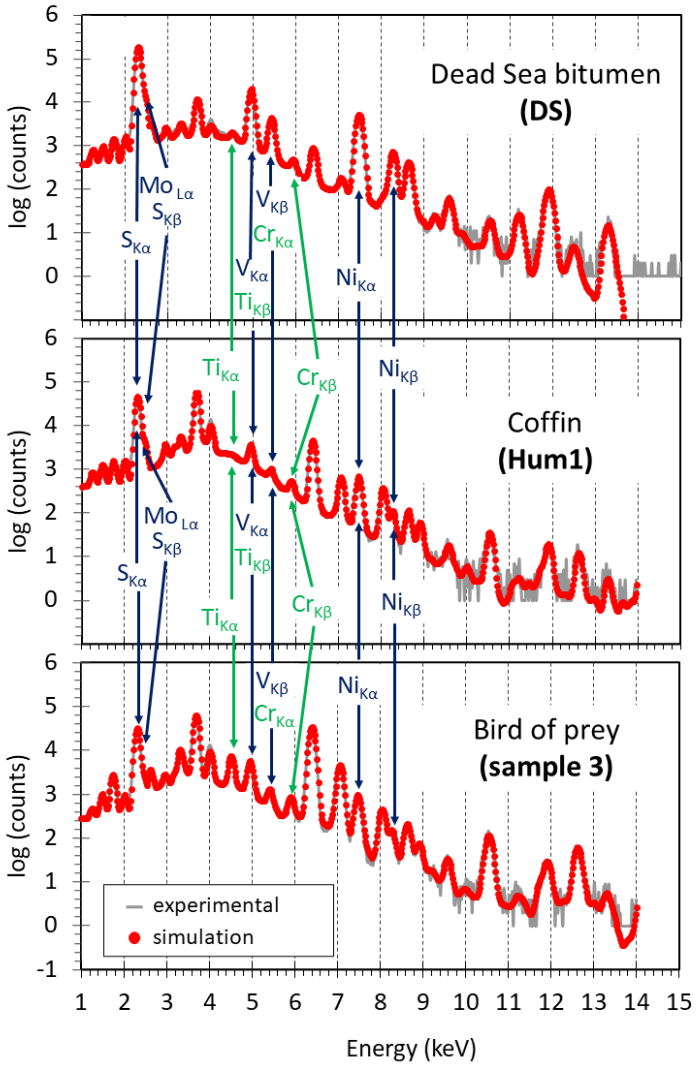

250

Fig. 2: three examples of PIXE spectra (grey line) with the Gaussian fit obtained with PyMCA (red points); the transitions of the bitumen marker elements S, V, Ni and Mo (blue) and Ti and Cr (green) are indicated.

255 Two observations can be made from this PIXE analysis. The first is that the presence of Ni and V enrichment indicates the presence of bitumen in all the samples, even in small quantities, and when GC-MS fails to detect it.[44] The second is that Ni and V concentrations appear to be linearly correlated (Fig. 3a). With the exception of sample 4 from corpus A, whose very low V and Ni contents are close to the sensitivity limit of the technique, all other data 260 points correspond to Ni:V ratios of between 1:2 and 1:4, with an average value of 1:3 (red line)

obtained by linear regression of corpuses A and B data. These Ni/V< 0.5 values indicate a marine origin of their source sediments (Ni/V between 1 and 10 indicate a lacustrine or terrestrial origin).[56] In principle, such a linear relationship between Ni and V contents should not be expected, unless the bitumens used for mummification have the same geological origin. Indeed, Ni and V do have not the same redox properties. During the settling of the dead biological matter to the sea floor, V^{V} and Ni^{II} ions present in the water form coordination complexes with humic and fulvic acids and other organic molecules until they reach the redox front near the water-sediment interface.[21,40,56] However, nickel remains in the Ni^{II} state as it traverses the redox front, while soluble V^{V} is reduced to insoluble V^{IV} (see Fig. S4). This means that Ni enrichment can be considered primarily as a marker of biomass productivity, while V enrichment is a marker of both biomass productivity and redox conditions at the sea floor. As a consequence, bitumen formed from organic sediments should have variable Ni and V contents with variable Ni:V ratios if these sediments were deposited in different aquatic environments (*i.e.* different redox conditions and biomass productivity).

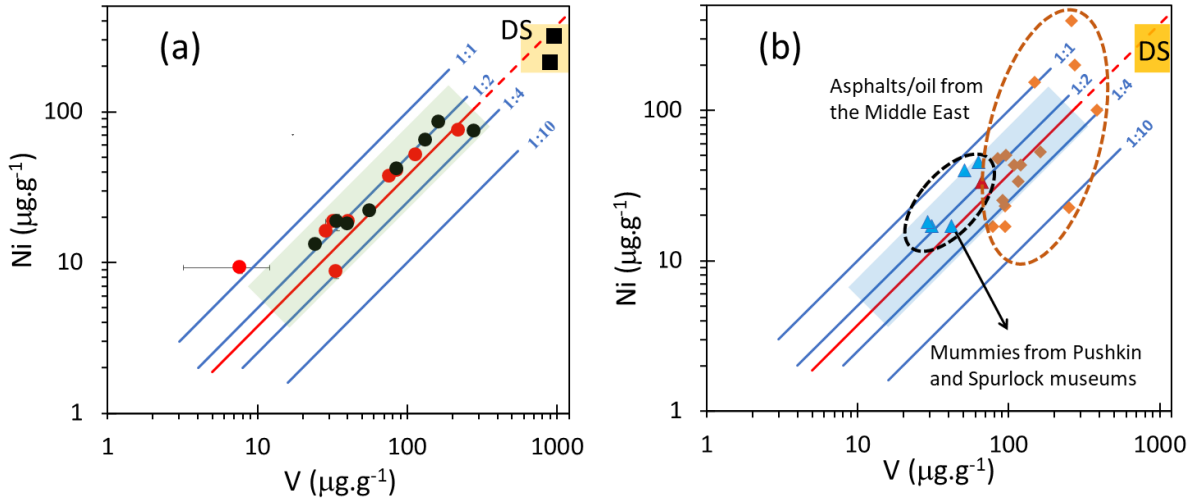

Fig. 3: Ni and V concentrations in (a) embalming matter of mummies of corpus A (red circles), corpus B (black circles) and in Dead Sea bitumen (black square); (b) embalming matter of human mummies from Pushkin and Spurlock museums (blue triangles) and asphalt/oil samples from the Middle East (brown diamonds). The blue lines are guides for the eyes, and correspond to different Ni:V ratios.

This variability in the Ni:V ratio as a function of the bitumen/oil source is illustrated in Fig.3b (data in Table S3), which represent the V and Ni contents of oil and bitumen from different sites in the Middle East,[57,58] It appears that they contain less V than the Dead Sea bitumen, and that their Ni contents are widely dispersed, resulting in a range of Ni:V ratios. Thus, the fact that Ni:V in the embalming matter of mummies of corpuses A and B is close to that of Dead Sea bitumen is a strong indication that their bitumen comes from the Dead Sea.

Figure 3b and Table S3 also show the V and Ni content of embalming matter from human mummies from the Pushkin Museum in Moscow, Russia, and the Spurlock Museum in Urbana, USA.[59,60] In the case of the Pushkin Museum mummies, the authors concluded that the bitumen originated from the Dead Sea.[59]

Table 2: Vanadium, nickel and molybdenum contents measured in nearly homogeneous areas selected from PIXE mappings of corpus A and B samples. Two mappings could be made on sample An2 and Hum2. Values in brackets for Mo have an error greater than 25%; in some cases, values are not mentioned when the error was 100% or when they could not be measured (*nm* = not measured).

		Concentration (μg.g^{-1})		
		V	**Ni**	**Mo**
Dead sea bitumen DS	DS(1)	888 ± 31	215 ± 12	62 ± 5
	DS(2)	953 ± 31	318 ± 17	98 ± 21
Corpus A	1	29 ± 2	16 ± 1	(11 ± 7)
	3	114 ± 4	52 ± 2	30 ± 6
	4	(8 ± 4)	9 ± 1	*nm*
	6	33 ± 2	9 ± 1	*nm*
	8	85 ± 4	41 ± 2	(14 ± 5)
	10	40 ± 2	19 ± 1	(8 ± 4)
	11	219 ± 8	76 ± 3	(15 ± 4)
	12	32 ± 4	19 ± 1	(14 ± 5)
	14	76 ± 4	37 ± 2	(18 ± 5)
Corpus B	An1	86 ± 3	42 ± 2	(12 ± 6)
	An2 (1)	133 ± 5	64 ± 3	(34 ± 9)
	An2 (2)	25 ± 2	13 ± 1	(7 ± 5)
	An3	281 ± 6	74 ± 2	19 ± 2
	An5	162 ± 8	85 ± 4	43 ± 7
	Hum1	56 ± 3	22 ± 1	(6 ± 3)
	Hum2 (1)	40 ± 3	18 ± 1	(3 ± 2)
	Hum2 (2)	34 ± 4	19 ± 2	*nm*

Assuming a Dead Sea origin for the bitumen in all the mummies of corpus A and B, its quantification in the black matter can be estimated by comparing their V and Ni contents with those of the DS samples. Considering that the V content of the DS bitumen is ≈ 1,000 μg.g^{-1}, and that the V content of the black matter of mummies ranges from 25 to 300 μg.g^{-1} for corpuses A and B, we can estimate that they contain between 3% and 30% bitumen. Using the same reasoning for the human mummies from the Pushkin and Spurlock museums, we can estimate that their black matter contains between 3% and 7% bitumen. These results are in line with ^{14}C analyses of 39 human mummies by Clark *et al.*[19], which showed that their embalming matter contains between 0 to 45% bitumen.

Molybdenum was more difficult to quantify by PIXE at trace levels, and the data are affected by large error bars (Table 2). Although Mo content was not measurable in some of our samples, the values obtained on samples from corpuses A and B, and those from published data for the Pushkin and Spurlock museums mummies, [59,60] are also consistent with a Dead Sea origin for the bitumen (see SI section S2.3).

EPR analysis of vanadyl complexes and organic radicals. A typical EPR spectrum of a bitumen sample from the Dead Sea (DS sample) is shown in Fig.4 (black line). It contains the two classic paramagnetic signatures of oil and bitumen: (i) an intense line with no apparent structure, representing polyaromatic hydrocarbon radicals labelled C^0 (~ 0.2×10^{18} spin.g^{-1}), characterized by a nearly free-electron *g*-value $g = 2.0037\pm0.0001$, and the classic spectrum of VO-P vanadyl porphyrin complexes (~ 3×10^{18} spin.g^{-1}) with two series of eight hyperfine transitions, many of which are difficult to detect (see Fig.S5 for the theoretical spectrum of VO-P). The EPR parameters deduced from the simulated spectrum are $g_{//} = 1.959\pm0.002$, $g_{\perp} = 1.980\pm0.002$, $A_{//} = 157(\pm3)\times10^{-4}$ cm^{-1} and $A_{\perp} = 54(\pm2)\times10^{-4}$ cm^{-1} for VO-P complexes.[44] Such an EPR spectrum with two types of paramagnetic molecules is typical of all petroleum asphaltenes from marine sediment kerogen.[43] In addition to these markers of bitumen, most samples of corpuses A and B showed a baseline distortion (Figs.4, S6 and S7), due to a very broad and unresolved ferromagnetic resonance signal revealing the presence of ferromagnetic iron oxide microparticles.[44]

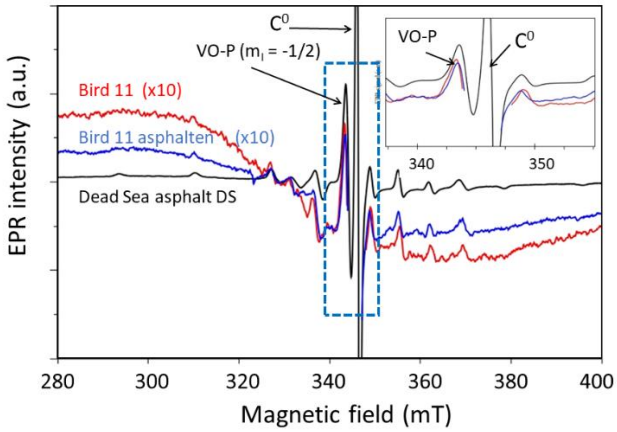

Fig. 4: EPR spectrum of a fragment of floating bitumen block from the Dead Sea (DS), in black, showing the single line of the hydrocarbon radicals C^0, and the multi-line spectrum of vanadyl porphyrin complexes VO-P; EPR spectrum of sample 11, in red, taken from a mummy of ibis (Late period) from Roda; The same sample after extraction in heptane, composed mainly of asphaltene, in blue; Microwave power 2 mW, modulation amplitude 0.2 mT.

Although much less intense, this characteristic spectrum was obtained in all the samples taken from the mummified birds of corpus A. An example is shown in Fig.4 for a fragment of black matter sampled on an ibis mummy from Roda (sample 11, see Fig.1 and Table S1). This EPR signature undoubtedly reveals the presence of bitumen. This type of EPR signal was observed for all the mummies of corpus A, and was more intense for the precipitate samples obtained after solvent extraction than for the raw samples (Fig.S6), showing that C^0 and VO-P species are mainly trapped in the asphaltene component of bitumen. In two cases (samples 4 and 5), even the sharp m_I = -1/2 hf line of VOP was too weak to be easily detected (see Fig.S6), suggesting that bitumen is absent from these samples. However, their asphaltene precipitates clearly showed the presence of both C^0 and VO-P signals, indicating a small amount of bitumen in these black matters. The same EPR signatures of bitumen were also observed in all samples from corpus B,[44] as shown in Fig. S7. VO-P (N_{VOP}) and C^0 (N_{C^0}) concentrations in embalming matter are generally higher in samples from corpus B than in those of corpus A (Table S.6 and Fig.5a), with N_{VOP} values ranging from ~ 0.25×10^{18} spin.g^{-1} to ~ 2.8×10^{18} spin.g^{-1} in corpus B, whereas they do not exceed ~ 0.5×10^{18} spin.g^{-1} in corpus A. This difference in bitumen content, also observed with PIXE measurements of V and Ni concentrations, may be explained by the need to save bitumen, a precious substance at the time, for bird mummies which were prepared in very large quantities.[6] Although C^0 radicals are in lower concentrations than VO-P, they can be easily detected as their EPR signal consists of a unique sharp transition, so that C^0 concentrations as low as ~ 10^{15} spin.g^{-1} can be measured.

The thermal history of embalming matters. The concentrations (N) of C^0 and VO-P in all samples from corpuses A and B are plotted in Fig.5a, which represents N_{C^0} versus N_{VOP} for raw samples (corpuses A and B) and for asphaltene precipitates (corpus A only). Two observations can be made from this diagram. Firstly, the fact that the precipitates are globally enriched in C^0 and VO-P compared with the raw samples confirms that these two types of paramagnetic molecules are predominantly located in the black matters, and more specifically in the asphaltene component of bitumen (Fig.5b is a zoom of Fig.5a for corpus A). Secondly, there is an apparent linear correlation between N_{C^0} and N_{VOP} for most samples, including asphaltene precipitates, except for sample 1 from corpus A, and samples An2/An3, An4 and Hum1 from corpus B (Fig.5a). With the exception of these samples, most of the experimental

points are very close to the line connecting the origin (absence of bitumen) and the value for pure Dead Sea bitumen (DS).

Such a linear correlation would not be expected for bitumen of different geological origins, as the concentrations of radicals C^0 and VO-P are controlled by independent physicochemical parameters. Indeed, VO-Ps are abundant in oil and bitumen when the original organic sediments have been deposited in an anoxic marine environment.[61] This is because vanadium V^V, always present in trace amounts (~ 39 nmol/L) as soluble vanadates (mainly $V_4O_{12}^{4-}$ and $V_2O_7^{4-}$ ions) in normally oxygenated marine water, is reduced to insoluble V^{IV} in the form of vanadyl VO^{2+} ions in the presence of abundant organic matter near the water/sediment interface.[21] During early diagenesis, these VO^{2+} ions are stabilized in organic-rich sediments by the substitution of Mg^{2+} and Fe^{2+} ions of porphyrin biomolecules (chlorophyll and hems), giving the stable VO-P complexes detected by EPR in oil and bitumen.[29,42,43] The enrichment in vanadium of fossil organic matter compared to seawater is the possible consequence of a pumping effect produced by the concentration gradient of soluble V^V near the water-sediment interface. Thus, the VO-P content of the source rock of bitumen is high (several hundreds of $\mu g.g^{-1}$) when the water reservoir is large (marine environment) and is much lower, or even absent, when the organic sediments have been deposited in a lacustrine or terrestrial environment.[56] The VO-P enrichment of bitumen reflects not only its marine origin, but also the acido-basic conditions (*pH*) and redox potential (*Eh*) of the source rock's depositional environment (see Fig.S4).[22,38,40,56]

Unlike VO-P, the C^0 polyaromatic hydrocarbon radicals are ubiquitous in all organic material, whether of biological or abiotic origin, transformed over geological time (tens of millions to billions of years)[46] or submitted to high temperatures (i.e up to 300 to 700°C).[62,63] They are present in coals,[64-66] in carbonaceous shales and cherts,[46,67] in petroleum oil,[68] and even in 4.5 Ga-old carbonaceous chondrites, the most primitive objects of the solar system.[69,70] As they possess an odd number of carbons, and thus a single electron in a highly delocalized molecular π-orbital, they give a characteristic EPR signal consisting of a single symmetrical line with no apparent structure and almost free-electron magnetic behavior.[45,62,64,71]

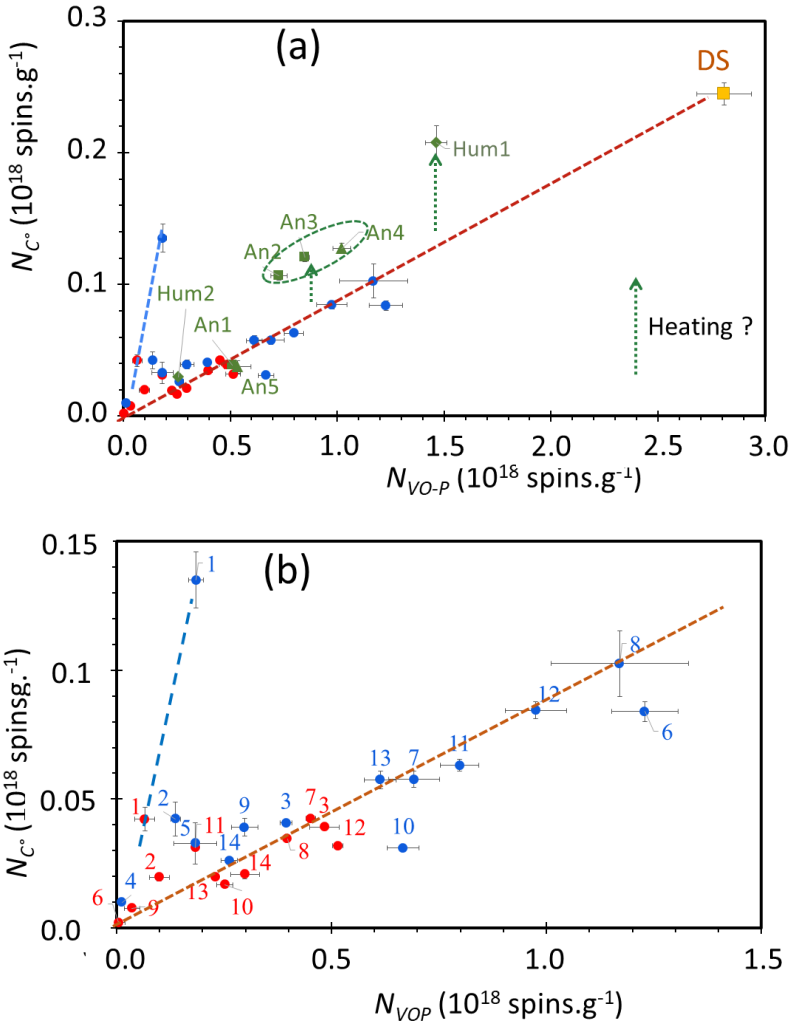

Fig. 5: Concentrations (in number of spins per g of material) of organic radicals C^0 and vanadyl porphyrins VO-P; (a) in the raw samples (red circles) and asphaltene precipitates (blue circles) for bird mummies from corpus A, and for animal (rams and crocodile) and human mummies from corpus B (green symbols) and Dead Sea bitumen DS (yellow square); (b) zoom from Fig.5a for the black matters from bird mummies and corresponding asphaltene precipitates.

Consequently, there are no genetic relationships between N_{C^0}, which depends on *T*, *P* and time *t* during burial, and N_{VOP} which depends mainly on *pH* and *Eh* and other parameters of the depositional environment. Therefore, bitumen samples from different marine environments (*pH* and *Eh*) and with different *P-T-t* histories during burial are not expected to show any correlation between their C^0 and VO-P concentrations. A linear relation (Eq.1) is expected for mummy black matter only in the specific case where it contains variable amounts

of bitumen from the same geological setting (i.e all parameters *pH*, *Eh*, *T*, *P* and *t* are identical):[44]

$$N_{C^0} = k\, N_{VOP} + N_{C^0}^{other} \quad (1)$$

where $N_{C^0}^{other}$ represents radicals in other heated or carbonized organic materials. The demonstration of Eq.1 is given in SI section 3.5. In the case of pure natural bitumen, we must have $N_{C^0}^{other} = 0$. The constant *k* in Eq.1 is characteristic of the source rock and geological setting of bitumen, *i.e* $k_{DS} = 8.6\times10^{-2}$ in the case of Dead Sea bitumen (broken red line in Fig.5a). With the exception of sample 1, the bird mummies from corpus A follow approximately the same linear behavior (Fig.5b). Similarly, samples Hum2, An1 and An5 from corpus B fit well with the characteristic line of Dead Sea bitumen (Fig.5a).

It appears that sample 1 from corpus A and samples An2/3 (the same ram mummy), An4 (crocodile mummy) and Hum1 (black matter from a human mummy) from corpus B deviate significantly from the characteristic line of Dead Sea bitumen (Fig.5a). This could suggest that the bitumen sources used for the embalming matter of these mummies are not from the Dead Sea. However, this hypothesis is at odds with the V, Ni and Ni/V values measured by PIXE, which indicate a Dead Sea origin for the bitumen of all these mummies. The most likely reason for the deviation of N_{C^0} and N_{VOP} values from the Dead Sea line could be heating of some components of the black matter before its application on the mummy, creating additional C^0 carbon radicals. The excess radicals produced by these heated organic matters are represented by the broken green lines in Fig.5a. According to Eq.1, the number of additional radicals is estimated by the vertical offset of the data points from the red line, $N_{C^0}^{other} \approx 0.6\times10^{17}$ spin.g^{-1} for An2, An3 and An4, and $N_{C^0}^{other} \approx 10^{17}$ spin.g^{-1} for Hum1.

Indeed, many EPR measurements on heat-treated biological materials (leaves, cyanobacteria, etc.) have shown that an intense C^0 signal appears as early as a 15-min treatment at 400°C.[62,72] By virtue of Arrhenius' law, which governs chemical reactions, the same concentration of radicals would be obtained by a short-term treatment t_a at a high temperature T_a and a longer treatment t_b at a lower temperature T_b:

$$t_a.\exp\left(-\frac{E}{kT_a}\right) = t_b.\exp\left(-\frac{E}{kT_b}\right) \quad (2)$$

On this basis, we can propose working hypotheses to explain the positive deviations from the Dead Sea line of several black matters in the C^0/VO-P diagram in Fig.5a. Three scenari can be envisaged from Eq.1: (i) If the bitumen has been strongly heated at high temperature before being mixed with the other organic substances of black matters, k is expected to increase without changing $N_{C^0}^{other}$; (ii) If a thermally treated organic material has been added to the mixture (bitumen + other organic substances), we expect an increase in $N_{C^0}^{other}$ without a change in k ; (iii) If all the black matters have been heated at high temperature before being applied to a mummy, both k and $N_{C^0}^{other}$ are expected to increase. Although there are only two experimental points for the anomalous sample 1 in corpus A, it could correspond to the first scenario because $N_{C^0}^{other} \approx 0$ and the value $k \approx 71\times10^{-2}$ is almost 10 times higher than for Dead Sea bitumen (k_{DS} = 8.6×10^{-2}). The data points for samples An2, An3 and An4, which appear almost aligned parallel to the characteristic line for Dead Sea bitumen (same slope k), would then have an intercept $N_{C^0}^{other} \approx 0.6\times10^{17}$ spin.g^{-1}, which corresponds to the second scenario (ii). All three situations remain possible for sample Hum 1, which is isolated from the other data in Fig. 5a. However, we can reasonably hypothesize that the black matters of Hum1, An2, An3 and An4 from corpus B contain some thermally treated organic matter in addition to Dead Sea bitumen.

The redox history of embalming matters. Potential-*pH* diagrams of the vanadium-oxygen and nickel-oxygen-sulfur systems at oceanic concentrations (Fig. S4) show that at a slightly alkaline *pH* (that of the present-day ocean is around 8), the redox stability domain of VO^{2+} (V^{IV} state) is narrow, favoring the formation of V^{III} species at a potential below -0.2 V and vanadate anions (V^{V} state) above -0.1 V.[40,61] Consequently, the redox conditions of marine organic sediments are compatible with the presence of the stable vanadium states V^{III}, V^{IV} and V^{V} states, while nickel is found only in the Ni^{II} state (grey areas in Fig. S4). PIXE spectroscopy enables the quantification of vanadium and nickel, but cannot distinguish between the V^{V}, V^{IV} and V^{III} states. EPR spectroscopy is specific to paramagnetic molecules, which is the case for VO^{2+} ions of VO-P complexes (V^{IV} state, d^1 configuration, $S = 1/2$). It has been shown that the one-electron reduction and oxidation of VO-P takes place not on the metal, but on the porphyrin ring, i.e. through the formation of $P^{-\bullet}$ and $P^{+\bullet}$ porphyrin radicals with spin $S = 1/2$.[73,74] As the VO^{2+} ion also has a spin $S = 1/2$, the latter interacts with the radical spin to form a singlet (S = 0) or triplet (S = 1) diradical. The singlet diradical is EPR-silent, and the triplet diradical has a large zero-field splitting (ZFS), so that only the $m_s = 0$ state is populated, and is also EPR-silent. Indeed,

it has been shown that the one-electron reduction or oxidation of VO-P causes the vanadyl EPR signal to disappear.[74]

Figure 6 and Table S7 show the comparison between the V^{IV} concentration (in the form of VO^{2+}) measured by EPR, and the total vanadium concentration $V^{total} = V^{III}+V^{IV}+V^{V}$ measured by PIXE. The red line in the diagram represents the limiting situation where all vanadium atoms are in the V^{IV} state of VO-P, corresponding to $(V^{IV}/V^{total})_{max} = 1$, and the blue area is the forbidden domain corresponding to $V^{IV}/V^{total} > 1$. Assuming that all vanadium atoms are in the form of VO^{2+} ions in VO-P complexes, we would expect all experimental points to lie on this line. However, it is clear that the experimental point for Dead Sea bitumen (DS) in Fig. 6 is considerably offset from the red line, indicating that about 74% of the vanadium is EPR-silent. This apparent deficit in paramagnetic V^{IV} relative to V^{total} may be explained by considering that vanadyl porphyrin complexes are present both as neutral VO-P (EPR active, 26%) and as EPR-silent $VO\text{-}P^{-}$ anions (74%). Although these anions are relatively unstable and reactive,[75] they could be stabilized and protected in the reducing network of the asphaltene component of bitumen in the form of $(VO\text{-}P)^{-}X^{+}$ ion pairs, X^{+} being a compensating cation as K^{+} for example, as this element is present in bitumen (see Table S5).

Assuming that the bitumen in the mummies' embalming matter originates from the Dead Sea, as the present PIXE and EPR analyses tend to show, we would expect the V^{IV}/V^{total} ratio to be conserved in absence of redox reactions. In this case, the experimental points for the studied mummies should be located close to the line connecting DS to the origin, characterized by $(V^{IV}/V^{total})_{DS} \approx 0.26 \pm 0.01$ (interrupted line in Fig.6). This trend was indeed observed for several samples (3, 8, 14, An3 and An5), but two samples from corpus A have very low V^{IV}/V^{total} value (0.01 for sample 6, and 0.07 for sample 11), and four samples (12, An1, An2 and Hum1) are closer to the maximum possible value $(V^{IV}/V^{total})_{max} = 1$ defined by the red line, with sample Hum1 clearly in the forbidden domain ($V^{IV}/V^{total} \approx 2.2$). The case of Hum1 is discussed in section S.6 of the SI. We propose that the scattering of several experimental points in the diagram of Fig. 6 is due to a change in the redox state of VO-P in the black matter, resulting from environmental weathering and/or bio-alteration during the long burial history of these mummies, which can vary from one mummy to another depending on the environmental conditions of the burial site.

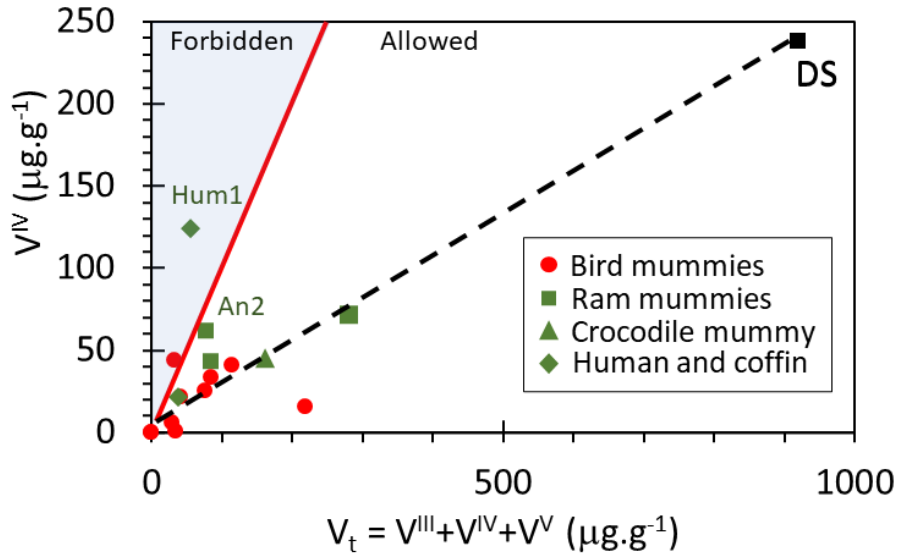

Fig. 6: Diagram showing V^{IV} concentrations (from EPR of VO^{2+} in VO-P) as a function of total vanadium concentrations V^{total} (from PIXE). The red line is the limit corresponding to $V^{IV}=V^{total}$, and the colored area represents the forbidden domain $V^{IV}>V^{total}$. The broken line links the origin to the Dead Sea bitumen data. The corresponding V^{IV} and V^{total} contents are shown in Table S7.

In this model, the presence of points far above or far below the DS line may be explained by a simple oxidation effect on the embalming matter. We hypothesized above that VO-P complexes in DS bitumen could be present in two forms: neutral VO-P (EPR-active) and VO-P^- anions (EPR-silent). If alteration has resulted in the oxidation of VO-P^- anions to neutral VO-P, this is equivalent to converting an EPR-silent species into EPR-active one, and thus increasing the EPR intensity of V^{IV} signal with respect to the DS line. This mechanism may explain the presence of experimental points close to the limit value $(V^{IV}/V^{total})_{max} = 1$. Alternatively, the one-electron oxidation of neutral VO-P occurs on the porphyrin ring, giving an EPR-silent VO-P^+ cation.[74] If alteration has produced the oxidation of neutral VO-P to VO-P^+ cation, this is equivalent to converting an EPR-active species into EPR-silent one, and thus decreasing the intensity of the EPR signal with respect to the DS line. These two opposing effects of oxidation on VO-P complexes could explain the dispersion of experimental points below and above the characteristic DS line $(V^{IV}/V^{total})_{DS} \approx 0.26$. Compared to the native DS bitumen, this model implies that severe oxidation of black matter would result in an apparent deficit of vanadyl (i.e $V^{IV}/V^{total} < (V^{IV}/V^{total})_{DS}$), while more moderate oxidation would result in an apparent excess of vanadyl (i.e $V^{IV}/V^{total} > (V^{IV}/V^{total})_{DS}$). This working hypothesis need to be tested by probing the oxidation states of vanadium, for example by synchrotron X-ray absorption spectroscopy (XAS),[76,77] or by the newly developed wavelength dispersive X-ray fluorescence (WDXRF), which has the advantage of being a non-synchrotron technique.[78]

Conclusion and perspective

We used PIXE and EPR analyses to investigate the potential of certain transition metals, in particular V, Ni and secondarily Mo, as indicators of the presence of bitumen and to trace its origin and alteration in embalming matter of Egyptian mummies. Transition metal elements are much more stable than degradable organic molecules, and V has several stable oxidation states, among which the paramagnetic V^{IV} state can be detected by EPR, providing information on the redox conditions prevailing throughout the material's history, from its origin to its degradation in mummies by weathering and/or bio-alteration.

This PIXE analysis showed that the embalming matter of all mummies studied in this work, which span a period of around 1000 years and come from different sites in Egypt, contain bitumen with a nearly constant Ni:V ratio. This constant metal ratio suggests a common source of bitumen supply, which is likely the Dead Sea. The same conclusion was deduced from the EPR of vanadyl porphyrins VO-P and carbon radicals C^0, with a concentration ratio C^0/VO-P for bird mummies close to that measured for DS bitumen, which also indicates the same source (Dead Sea) for the bitumen used for these mummies. The presence of excess carbon radicals in the embalming matter of several mummies indicates that, in addition to bitumen and other biological substances, they may contain thermally-treated, or carbonized, organic matter. The relatively low bitumen content of the embalming matter of birds compared with other human and animal mummies suggests that these massive bird mummifications were practiced on a quasi-industrial scale in ancient Egypt, with a precise source of bitumen supply, and probably a fabrication recipe specific to this type of mummy.

This combined EPR-PIXE methodology is both quantitative and sensitive, since a few % of bitumen can be non-destructively detected in a sample weighing just a few mg. The combination of these two techniques also provides information on the thermal history (preparation recipes) and redox history (degradation) of these black matters.

In principle, EPR can be used on-site (in museums), as lightweight, low-volume, air-cooled EPR spectrometers are commercially available, requiring only a power supply. Together with X-ray fluorescence spectroscopy (XRF), which is also a mobile technique, EPR can therefore be used as a rapid method for detecting the presence of dead carbon prior to ^{14}C dating.

Data availability

All EPR and PIXE spectra, and the data supporting this article have been included as part of the ESI.

Author contributions

OA: EPR and PIXE experiments and data curation; DG: Conceptualization, methodology, PIXE analyses, writing original draft, review and editing; LB: methodology, EPR and PIXE analyses, validation; AM: Preparation of asphaltene precipitates; VG: Provision of studied samples and preparation of asphaltene precipitates, validation; ALD: Project administration, validation.

Conflict of interest

There are no conflicts of interest to declare

Acknowledgments

Didier Berthet (Musée des Confluences, Lyon) and Romain Amiot (LGL-TPE) are gratefully acknowledged for allowing us to access the Museum collection and guiding us in the sampling of certain mummies, respectively. The authors thank Quentin Lemasson, Laurent Pichon and Thomas Calligaro from C2RMF and AGLAE facility, Paris, France, for their help in carrying out the PIXE analyses and processing the data. Apichai Manaprasertsak is sincerely thanked for his help and contribution to the EPR dosimetry. Pascale Richardin (C2RMF) is thanked for the ^{14}C dating of certain mummies.

REFERENCES

1 J.C. Goyon, Rituels funéraires de l'ancienne Egypte, *Littérature ancienne du Proche-Orient 4*, 1997, Les éditions du cerf.

2 S. Schiødt, *Medical Science in Ancient Egypt: A translation and interpretation of Papyrus Louvre-Carlsberg*. PhD thesis, 2021, University of Copenhagen.

3 A. Marshall, and R. Lichtenberg, *Les momies égyptiennes : La quête millénaire d'une technique*. 2013, Paris: Fayard.

4 K. Fulcher, M. Serpico, J.H. Taylor, and R. Stacey, *Proc. Nat. Acad. Sci (USA)*, 2021, **118**, e2100885118. https://doi.org/10.1073/pnas.2100885118

5 S. Bussi, S. Economie du culte des animaux sacrés en Egypte hellénistique et romaine. In *Creatures of Earth, Water, ans Sky : Essays on animals in Ancient Egypt and Nubia*, Ed. Porcier S. *et al*., Sidestone Press, 2019, 119-126.

6 M. Linglin, R. Amiot, P. Richardin, S. Porcier, I. Antheaume, D. Berthet, V. Grossi, F. Fourel, J-P. Flandrois, A. Louchart, J.E. Martin, and C. Lécuyer, *Scientific Reports*. 2020, **10**, 15463. https://doi.org/10.1038/s41598-020-72326-7.

7 S.A. Buckley, and R.P. Evershed, *Nature*, 2001, **413**, 837-41. https://doi.org/10.1038/35101588.

8 M. Ménager, C. Azémard, and C. Vieillescazes, *Microchem. J.* 2014, **114**, 32-41. https://doi.org/10.1016/j.microc.2013.11.018.

9 J. Lucejko, J. Connan, S. Orsini, E. Ribechini, F. Modugno, *J. Archaeolog. Sci*. 2017, **85**, 1-12. https://doi.org/10.1016/j.jas.2017.06.015

10 R. Brettell, W. Martin, S. Atherton-Woolham, B. Stern, and L. McKnight, *Studies in Conservation*, 2017, **62**, 68-82. https://doi.org/10.1179/2047058415Y.0000000027.

11 J. Jones, F.G. Higham, D. Chivall, R. Bianucci, G.L. Kay, M.J. Pallen, R. Oldfield, F. Ugliano, and S.A. Buckley, *Journal of Archaeological Science*, 2018, **100**, 191-200. https://doi.org/10.1016/j.jas.2018.07.011.

12 M.P. Colombini, F. Modugno, F. Silvano, and M. Onor, *Stud. Conserv*. 2000, **45**, 19-29. https://doi.org/10.1179/sic.2000.45.1.19.

13 J. Hertzog, H. Fujii, R. Zostautaite, A. Lattuati-Derieux, P. Richardin, V. Carré, F. Aubriet, and P. Schmitt-Kopplin, *Journal of Archaeological Science: Reports*, 2022, **48**, 103861-70. https://doi.org/10.1016/j.jasrep.2023.103861.

14 M.M Wright, and B.B. Wheals, *Journal of Analytical and Applied Pyrolysis*, 1987, **11**, 195-211. https://doi.org/10.1016/0165-2370(87)85028-3.

15 J.S. Mills, and R. White, *Archaeometry*, 1989, **31**, 37-44. https://doi.org/10.1111/j.1475-4754.1989.tb01054.x

16 M. Ferrant, I. Caffy, R. Cortopassi, E. Delque-Kolic, H. Guichard, C. Mathe, C. Thomas, C. Vieillecazes, L. Bellot-Gurlet, and A. Quiles, *J. Cult. Herit.* 2022, **55**, 369-380. https://doi.org/10.1016/j.culher.2022.04.007.

17 J. Maurer, T. Möhring, J. Rullkötter, and A. Nissenbaum, *Journal of Archaeological Science*, 2002, **29**, 751-62. https://doi.org/10.1006/jasc.2001.0773.

18 S.A Buckley, K.A. Clark, and R.P. Evershed, *Nature*, 2004, **43**, 294−298. https://doi.org/10.1038/nature02849

19 K.A Clark, S. Ikram, and R.P. Evershed, *Philos. Trans. R. Soc. A*, 2016, **374**, 20160229. https://doi.org/10.1098/rsta.2016.0229.

20 M. Rageot, R.B. Hussein, S. Beck, V. Altmann-Wendling, M.I.M. Ibrahim, M.M. Bahgat, A.M. Yousef, K. Mittelstaedt, J.J. Filippi, S. Buckley, C. Spiteri, and P.W. Stockhammer, *Nature*, 2023, **614**, 287-293. https://doi.org/10.1038/s41586-022-05663-4.

21 G.N. Breit, and R.B. Wanty, *Chem. Geol*. 1991, **91**, 83-97. https://doi.org/10.1016/0009-2541(91)90083-4.

22 N. Tribovillard, T.J. Algeo, T. Lyons, and A. Riboulleau, *Chem. Geol*. 2006, **232**, 12-32. https://doi.org/10.1016/j.chemgeo.2006.02.012.

23 J.F. Hein, *Journal of Petroleum Science and Engineering*, 2017, **154**, 551-563. https://doi.org/10.1016/j.petrol.2016.11.025

24 F. Baudin, N. Tribovillard, and J. Trichet, *Géologie de la matière organique*. 2e édition. 2017, EDP Sciences.

25 M. Mastalerza, A. Drobniaka, and A.B. Stankiewicz, *International Journal of Coal Geology*, 2018, **195**, 14–3. https://doi.org/10.1016/j.coal.2018.05.013

26 G. Ourisson, and P. Albrecht, *Accounts of Chemical Research*, 1992, **25**, 398-402. https://doi.org/10.1021/ar00021a003.

27 A. Lucas, A. *The Journal of Egyptian Archaeology*, 1914, **1** (4), 241-45. https://doi.org/10.2307/3853770.

28 P.E. Spielmann, *Journal of Egyptian Archaeology*, 1932, **18**, 177.

29 J. Rullkötter, and A. Nissenbaum, *Naturwissenschaften*, 1988, **75**, 618-21. https://doi.org/10.1007/BF00366476.

30 A. Lucas, and J.R. Harris, *Ancient Egyptian Materials and Industries, 4e Edition*. 1989, Histories and Mysteries of Man. London.

31 J.A. Harrell, and M.D. Lewan, *Archaeometry*, 2002, **44**, 285-93. https://doi.org/10.1111/1475-4754.t01-1-00060.

32 E. Davies, *Chemistry World*, 2011, **8**: 48-51.

33 J. Connan, *Le bitume dans l'Antiquité*. 2012, Paris: Editions Errance.

34 P. Wilde, T.W. Lyons, and M.S. Quinby-Hunt, *Chem. Geol*. 2004, **206**, 167-176. https://doi.org/10.1016/j.chemgeo.2003.12.005.

35 F. Galarraga, K. Reategui, A. Martinez, J.F. Llamas, and G. Marquez, *Journal of Petroleum Science and Engineering*, 2008, **61**, 9-14. https://doi.org/10.1016/j.petrol.2007.10.001.

660 36 T.J. Algeo, and T.W. Lyons, *Paleoceanography*, 2006, **21**, 1-23. https://doi.org/10.1029/2004PA001112.

37 O.H. Ardakani, R. Hlohowskyi, A. Chappaz, H. Sanei, M.H. Liseroudi, and J.M. Wood, *Geochim. Cosmochim. Acta*, 2020, **283**, 136-148. https://doi.org/10.1016/j.gca.2020.06.006.

38 L. López, and S. Lo Mónaco, *Organic Geochemistry*, 2017, **104**, 53-68.
665 https://dx.doi.org/10.1016/j.orggeochem.2016.11.007.

39 P. Sundararaman, and R.J. Hwang, *Geochim. Cosmochim. Acta*, 1993, **57**, 2283-2290. https://doi.org/10.1016/0016-7037(93)90569-I.

40 M.D. Lewan, *Geochim. Cosmochim. Acta*, 1984, **48**, 2231-2238. https://doi.org/10.1016/0016-7037(84)90219-9.

670 41 P. Sundaramanan, and C.J. Boreham, *Geochim. Cosmochim. Acta*, 1993, **57**, 1367-1377. https://doi.org/10.1016/0016-7037(93)900-78-B

42 E.W. Baker, and J.W. Louda, *Biological Markers in the Sedimentary Record*; R.B. John, Ed.; Elsevier: Amsterdam, Netherlands. 1986, pp 125−225.

43 P.I. Premovic, I.R. Tonsa, M.S. Pavlovic, L. Lopez, and S. LoMonaco, *Fuel*, 1998,
675 **77**(15), 1769-1776. https://doi.org/10.1016/S0016-2361(98)00100-8.

44 C.E. Dutoit, L. Binet, H. Fujii, A. Lattuati-Derieux, and D. Gourier, *Anal. Chem*. 2020, **92**, 15445-15453. https://dx.doi.org/10.1021/acs.analchem.0c03116.

45 C.E. Dutoit, L. Binet, H. Vezin, O. Anduze, A. Lattuati-Derieux, and D. Gourier, *Magn. Reson*. 2022, **3**, 111-124. https://doi.org./10.5194/mr-3-111-2022.

680 46 A. Skrzypczak-Bonduelle, L. Binet, O. Delpoux, H. Vezin, S. Derenne, F. Robert, and D. Gourier, *Appl. Magn. Reson*. 2008, **33**, 371-397. https://doi.org/10.1007/s00723-008-0083-y.

47 P. Richardin, Rapport de datation par le carbone 14 de momies d'ibis et de rapaces, Projet ISOTHOT, Rapport N° 40965. 2019, C2RMF, Paris

685 48 P. Richardin, P. Rapport de datation par le carbone 14 de momies d'ibis et de rapaces du Musée des Confluences, 2022, Rapport N° 48470. C2RMF, Paris.

49 A. Nissenbaum, and S. Buckley, *Archaeometry*. 2013, **55**, 563-568. https://doi.org/10.1111/j.1475-4754.2012.00713.x .

50 M.K. Jones, D.E.G. Briggs, G. Eglinton, and E. Hagelberg, *Philos. Trans. R. Soc. B*,
690 1999, 354, 3-5. https://doi.org/10.1098/rstb.1999.0355.

51 C.G. Ryan, *Nucl. Instr. and Meth. B*, 1995, **104**, 377-394. https://doi.org/10.1016/0168-583X(95)00390-8

52 L. Pichon, B. Moignard, Q. Lemasson, C. Pacheco, and Ph. Walter, *Nucl. Instrum. Methods* B, 2014, **318**, 27-31. https://doi.org/10.1016/j.nimb.2013.06.065.

53 V.A. Sole, E. Papillon, M. Cotte, Ph. Walter, and J. Susini, *Spectrochim. Acta, Part B*, 2007, **62**, 63-68. <http://pymca.sourceforge.net>. https://doi.org/10.1016/j.sab.2006.12.002

54 L. Pichon, T. Calligaro, Q. Lemasson, B. Moignard, and C. Pacheco, *Nucl. Instrum. Methods* B, 2015, **363**, 48-54. https://dx.doi.org/10.1016/j.nimb.2015.08.086

55 S. Stoll, and A. Schweiger, *J. Magn. Reson*. 2006, **178**, 42-55. https://doi.org/10.1016/j.jmr.2005.07.012.

56 A.J.G Barwise, *Energy Fuels*, 1990, **4**, 647-652. https://doi-org.inc.bib.cnrs.fr/10.1021/ef00024a005.

57 R.F. Marschner, and H.T. Wright, *Archaeological Chemistry-II*, 1978, **171**, 150-171. https://doi.org/10.1021/ba-1978-0171.ch010

58 G.G. Benson, S.R. Hemingway, and F.N. Leach, The analysis of the wrappings of mummy 1770, In *The Manchester Museum Mummy Project: Multidisciplinary Research on Ancient Egyptian Mummified Remains*, 1979, 119-132. Manchester: Manchester Museum.

59 E.B. Yatsishina, V.M. Pozhidaev, Ya.E. Sergeeva, V.M. Retivov, E.Yu. Tereshchenko, I.S. Kulikova, and E.I. Panarina, E.I. *J. Anal. Chem*. 2021, **76**, 779-784. https://doi.org/10.1134/S1061934821040122

60 M.L. Proefke, and K.L. Rinehart, *J. Am. Soc. Mass. Spectrom.* 1992, **3**, 582-589. https://doi.org.inc.bib.cnrs.fr/10.1016/1044-0305(92)85036-J

61 J-H. Huang, F. Huang, L. Evans, and S. Glasauer, *Chem. Geol*. 2015, **417**, 68-89. http://dx.doi.org/10.1016/j.chemgeo.2015.09.019

62 S. Mrozowski, *Carbon*, 1988, **26**, 531-541. https://doi.org/10.1016/0008-6223(88)90152-2.

63 M. Bourbin, D. Gourier, S. Derenne, L. Binet, Y. Le Du, F. Westall, B. Kremer, and P. Gautret, *Astrobiology*, 2013, **13**, 151-162. https://doi.org/10.1089/ast.2012.0855.

64 J. Uebersfeld, A. Etienne, and J. Combrisson, *Nature*, 1954, **174**, 614. https://doi.org/10.1038/174614a0.

65 H.L. Retcofsky, G.P. Thompson, R. Raymond, and R.A. Friedel, *Fuels*, 1975, **54**, 126-128. https://doi.org/10.1016/0016-2361(75)90068-X.

66 J.K. Whelan, and C. Thompson-Rizer, In *Organic Geochemistry*, edited by M. Engel and S. Macko, 1993, Plenum Press, New York, 289-353.

67 J.M. Rigali, and B. Nagy, *Geochim. Cosmochim. Acta*, 1997, **61**, 357-368. https://doi.org/10.1016/S0016-7037(96)00334-1.

68 T.F. Yen, and S.R. Sprang, *Geochim. Cosmochim. Acta*. 1977, **41**, 1007-1018. https://doi.org/10.1016/0016-7037(77)90096-5.

69 L. Binet, D. Gourier, S. Derenne, and F. Robert, *Geochim. Cosmochim. Acta*, 2002, **66**, 4177-4186. https://doi.org/10.1016/S0016-7037(02)00983-3.

70 O. Delpoux, D. Gourier, H. Vezin, L. Binet, S. Derenne, and F. Robert, *Geochim. Cosmochim. Acta*. 2011, **75**, 326-336. https://doi.org/10.1016/j.gca.2010.09.033.

71 T.A. Dickneider, S. Scull, J.K. Whelan, and N.V. Blough, *Org. Geochem*. 1997, **26**, 341-352. https://doi.org/10.1016/S0146-6380(97)00010-7.

72 M. Bourbin, S. Derenne, D. Gourier, J.-N. Rouzaud, P. Gautret, and F. Westall, *Orig. Life. Evol. Biosph*. 2012, **42**, 569–585. https://doi.org/10.1007/s11084-012-9320-3.

73 P. Hambright, P. Neta, M.-C. Richoux, Z. Abou-gamra, and A. Harriman, *Journal of Photochemistry*, 1987, **36**, 255-265. https://doi.org/10.1016/0047-2670(87)80017-5.

74 C.M. Newton, and D.G. Davis, *J. Magn. Reson*. 1975, 20, 446-457. https://doi.org/10.1016/0022-2364(75)90002-5.

75 D. Shimizu, and A. Osuka, *Chem. Sci*. 2018, **9**, 1408-1423. https://doi.org/10.1039/c7sc05210c

76 G. Caumette, C.-Ph. Lienemann, I. Merdrignac, B. Bouyssiere, and R. Lobinski, *J. Anal. At. Spectrom*. 2009, **24**, 263-276. https://doi.org/10.1039/b817888g

77 G.S. Silversmit, H. Poelman, I. Sack, G. Buyle, G.B. Marin, and R. De Gryse, *Catalysis Letters*, 2006, **107**, 61-71. https://doi.org/1011-372X/06/0200-0061/0

78 E.P. Jahrman, G.T. Seidler, and J.R. Sieber, *Anal. Chem*. 2018, **90**, 6587-6593. https://doi.org/10.1020/acs.analchem.8b00302 .